communications earth & environment

Article

https://doi.org/10.1038/s43247-024-01812-x

Enhanced stratosphere-troposphere and tropics-Arctic couplings in the 2023/24 winter

Check for updates

Lu Qian [1,2], Jian Rao [1] ✉, Rongcai Ren [1,3], Chunhua Shi [1] & Siming Liu [4]

The stratosphere-troposphere and the tropics-Arctic couplings were intermittently enhanced in the 2023/24 winter. Here we used ERA5 reanalysis data and found that due to the amplification of planetary wavenumber 1 and 2 pulses, three displacement-type sudden stratospheric warming events occurred in one winter under the background conditions of warming equatorial middle and east Pacific, active equatorial convections, and easterly stratospheric equatorial winds. During the sudden stratospheric warming events, the stratospheric disturbances propagated downward to the surface, followed by continental cold surges. The residual meridional circulation was strengthened across the tropics and Arctic, anomalously more water vapor was transported into the stratosphere in tropics, while ozone content diminished in the lower stratosphere and grew in the upper stratosphere over the tropics. Meanwhile, water vapor and ozone over the Arctic exhibited a dipping pattern from the upper to the lower stratosphere.

The sudden stratospheric warming (SSW) is the most spectacular phenomenon of the stratospheric polar vortex[1–3]. Tropospheric Rossby waves can propagate upwards into the high-latitude stratosphere and dissipate, disturbing the polar vortex in the stratosphere[4,5]. The temperature in the polar stratosphere rapidly rises by tens of Kelvins within a few days, and the corresponding westerly winds in the polar region suddenly decelerate[6]. When the temperature gradient in the polar region reverses and westerly wind at 10hPa/60°N changes to easterly wind, it is recognized as a major SSW[1,6,7]. If the westerly wind does not change to easterly, it is defined as a minor SSW[1,6]. Major SSWs occur 6 or 7 times every 10 years in the Arctic and very few occur in the Antarctic[8–12]. According to the polar vortex geometry, displacement and split polar vortex are two types of SSWs[9,13]. Displacement SSW is characterized by the polar region occupied by the high center during the SSW eruption, while the polar vortex deviates from the North Pole to one side[1,2,9,13]. The split type of SSW is identified as the polar vortex splitting into two smaller ones and moving towards two sides of the hemisphere during the SSW onset[1,9,13,14]. Typically, displacement SSW and split SSW are associated with disturbances of planetary wavenumber 1 and 2, respectively[15–17]. During the SSW, there was a clear stratosphere-troposphere coupling, accompanied by a ring-like pattern in the stratosphere, similar to the negative phase of the Northern Annular Mode (NAM)[18–20]. As the NAM signal gradually propagates downwards, the Arctic Oscillation in the troposphere develops towards the negative phase[21], and there is a considerable rise in the likelihood of continental-scale cold air activity[2,22–26]. Moreover, the downward propagation of the negative NAM signal related to SSW also affects the atmospheric diffusion conditions in the boundary layer and modulates the sub-seasonal variation of $PM_{2.5}$ concentration[27–30].

The Brewer–Dobson (BD) circulation links the polar and tropical regions of the stratosphere with a meridional-vertical flow, and it is an important route for tropics-Arctic coupling in the stratosphere[31–33]. The accumulation of eddy heat flux is the main driving force for the BD circulation, also known as the residual circulation[34,35]. The BD circulation rises from the tropics into the stratosphere and then sinks into the troposphere outside the tropics, which plays a major role in the transport of materials between the stratosphere and the troposphere[33,36]. During SSW occurrence, due to the enhancement of tropospheric planetary waves, the eddy heat flux pulse increases and the BD circulation is greatly enhanced[37,38]. The air mass rising from the troposphere through the BD circulation in the tropics experiences the freezing and drying process of water vapor in the low-temperature region near the tropopause, which directly affects the distribution of stratospheric water vapor[39,40]. The change of BD circulation

[1]Key Laboratory of Meteorological Disaster, Ministry of Education (KLME) / Joint International Research Laboratory of Climate and Environment Change (ILCEC) / Collaborative Innovation Center on Forecast and Evaluation of Meteorological Disasters (CIC-FEMD), Nanjing University of Information Science and Technology, Nanjing, China. [2]China Meteorological Administration Xiong'an Atmospheric Boundary Layer Laboratory, Xiong'an New Area, China. [3]State Key Laboratory of Numerical Modeling for Atmospheric Sciences and Geophysical Fluid Dynamics, Institute of Atmospheric Physics, Chinese Academy of Sciences, Beijing, China. [4]Department of the Geophysical Sciences, University of Chicago, Chicago, USA. ✉e-mail: raojian@nuist.edu.cn

during SSW also affects the stratospheric temperature structure in the tropical region, which thus influences the distribution of local ozone and water vapor[36,39]. The BD circulation sinks in the extratropics, transporting high-concentration water vapor and ozone from the upper to lower stratosphere in high latitudes. The BD circulation completes the source-sink cycle of ozone and water vapor in the stratosphere as it crosses the stratosphere and enters the troposphere over both poles[33,34,38,40].

The occurrence of SSW is modulated by several climate factors[41]. The stratospheric quasibiennial oscillation (QBO) is the dominant driving force for the interannual variability in the tropical stratosphere, which is featured by cycling alternations between easterly and westerly winds on average every 28 months[42,43]. The QBO can modulate the position of the zero wind speed contour, thereby changing the waveguide that allows planetary waves to propagate upwards in the troposphere[43–45]. During the eastern QBO, the zero wind speed contour moves towards the subtropical region, and the wave activity towards the Arctic increases, which leads to weakening of the stratospheric polar vortex[43,45,46]. Changes in the thermal conditions in different ocean regions can trigger or amplify tropospheric planetary waves, which then propagate upwards to modify the strength of the stratospheric polar vortex[2,41,43,47]. Specific Madden–Julian Oscillation (MJO) phases and increased MJO amplitudes are beneficial for triggering planetary wave activities in subtropical regions[2,41,48]. El Niño-Southern Oscillation (ENSO) exhibits asymmetry in affecting the intensity of stratospheric polar vortex, with both El Niño and La Niña favorable for increased probability of SSWs[43,47]. Sea ice changes in the Barents-Kara Sea (BK) can enhance climate planetary waves, and BK sea ice loss has a unique role in triggering disturbance of the stratospheric polar vortex[49–51].

In early 2024, the Arctic stratospheric polar vortex experienced severe disturbances, with two major SSWs and one minor SSW in quick succession, which were more intense than those in the 2022/23 winter. In the past three decades, such frequent and violent changes in the Arctic stratospheric polar vortex have been quite rare. The atmospheric and oceanic environment in the 2023/24 winter was also very different from that in 2022/23[52]. Therefore, the SSW events in early 2024 merit thorough investigation. This paper provides a detailed analysis from three perspectives: stratosphere-troposphere coupling, tropics-Arctic coupling, and the background atmospheric and oceanic environment.

Results

Stratosphere-troposphere coupling during three SSWs in early 2024

Figure 1 shows the stratospheric polar vortex disturbances in the Arctic from mid-December in 2023 to the beginning of April in 2024, with four noticeable westerly decelerations, three of which shifted to easterlies, as marked by vertical lines. During the first easterly disturbance, the average zonal wind speed at 60°N on 16 January was −1 m/s and lasted for only 2 days (Fig. 1a), while in the Arctic circle, the temperature gradient turned positive (Fig. 1d), which is a marginal major SSW. However, easterly anomalies at 80°N lasted for 8 days from 13 January, and the zonal-mean air temperature at 80°N was 15 K higher than that at 60°N. The second easterly disturbance occurred on 16 February,

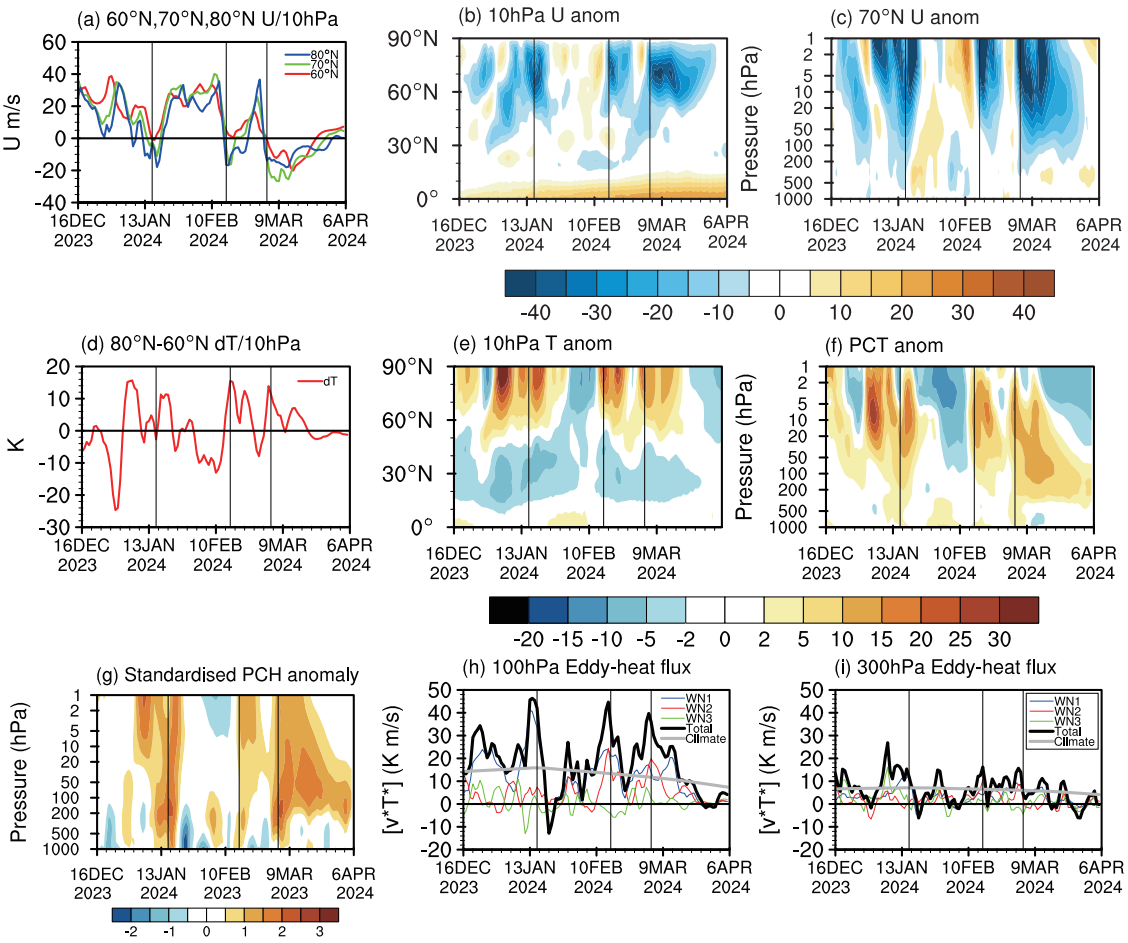

Fig. 1 | Spatiotemporal evolutions of the stratospheric circulation from 16 December 2023 to 6 April 2024. a Zonal-mean zonal winds at three latitudes (unit: m s^{-1}). **b** Zonal-mean zonal wind anomalies at 10 hPa (unit: m s^{-1}). **c** Zonal wind anomalies at 60°N (unit: m s^{-1}). **d** Zonal-mean temperature difference between 80°N and 60°N (unit: K). **e** Zonal-mean temperature anomalies at 10 hPa (unit: K). **f** Arctic polar cap temperature anomalies (unit: K). **g** Normalized polar cap geopotential height anomalies. **h** Eddy heat flux averaged from 45°N to 75°N at 100 hPa (unit: K m s^{-1}). **i** As in (**h**), but for 300 hPa. The vertical lines indicate the date when the zonal-mean westerlies reversed to easterlies.

when the westerlies at three latitudes rapidly weakened simultaneously and the westerlies at 70°N (4 days) and 80°N (8 days) turned to easterlies, and the zonal-mean air temperature at 80°N was 14 K higher than that at 60°N. The third easterly disturbance occurred on 4 March, with westerlies rapidly weakening and reversing to easterlies at three latitudes. The easterlies lasted for 21 days at 60°N and 29 days at 80°N, and reached a maximum of 24 m s^{-1} at 70°N. The zonal-mean air temperature at 80°N was 10 K higher than that at 60°N. The westerlies at 60°N reversed to easterlies, which persisted for more than 5 days in late March. The third disturbance was a major SSW rather than a spring final warming event[1,6]. Three SSWs occurred unprecedently in one winter, which has not been recorded in the last 30 years[52]. The frequent stratospheric polar vortex disturbances may be attributed to a sustained strong but intermittent dynamical forcing, which overwhelmed the diabatic cooling effect this winter.

According to the temporal evolution of the 10 hPa zonal-mean zonal wind anomalies (Fig. 1b), it was observed that the easterly anomalies during the first disturbance appeared in the North Pole and propagated southward to 40°N, and the easterly anomalies reached the maximum of 35 m s^{-1} on January 16. The second easterly anomalies began to form on 16 February, with a maximum value of 30 m s^{-1}. The third easterly disturbance began on 4 March and lasted until the end of March, with the largest easterly anomalies of 40 m s^{-1}. The zonal-mean zonal wind anomalies at 70°N are largest in the upper stratosphere (Fig. 1c). Two centers (~−40 m s^{-1}) appeared before and after the first disturbance, respectively, resulting in a long time of easterly anomalies and propagation downward to 500 hPa. The second easterly disturbance only propagated downward to 50 hPa, failing to reach the troposphere. The third disturbance propagated downward to the troposphere (500 hPa), reaching a maximum of −40 m s^{-1} around 5 March and lasting until the end of March.

Evolution of the temperature anomalies was similar to the change of the easterly anomalies, and all the three disturbances showed corresponding warm anomalies, with the latitude range from the North Pole to 60°N and even more southward (Fig. 1e). During the first disturbance, the warm anomalies had two maximum centers (~30 K) before and after the SSW onset, respectively, resulting in a long impact period of more than 30 days. The second disturbance was almost contiguous with the third disturbance, while the anomaly magnitude was weaker than that of the first disturbance. From the pressure-temporal evolution of the Arctic temperature anomalies (Fig. 1f), it was found that the strongest warm anomalies center (~30 K) appeared at 5–10 hPa before the first disturbance, and the temperature anomalies during all the three disturbances propagated downward to the troposphere. The zonal mean temperature anomalies of the first and third disturbances (major SSW) developed to the ground, and the temperature anomalies of the second disturbance mainly developed above 200 hPa.

As a representative of the NAM index, the standardized geopotential height anomalies in the Arctic region exhibited obvious downward propagation to the near surface, especially during the first and third disturbance periods (Fig. 1g). Positive height anomalies appeared in the stratosphere 14 days before the first SSW eruption, which propagated downward to the near surface five days before the SSW eruption and then lasted for 10 days. After the second and third SSW onsets, the stratospheric positive height anomaly signals appeared almost simultaneously with the near surface signals. The second positive height anomalies were short-lived, while the third positive anomalies persisted until April. It can be seen that the stratospheric signal had a relatively large impact on the near surface layer in early 2024.

Previous studies have shown that tropospheric planetary wave activities can propagate upward and weaken the stratospheric polar vortex, leading to onset of SSW events[16,17]. Eddy heat fluxes almost proportional to vertical component of the E-P flux are diagnosed in Fig. 1h, i for 100 hPa and 300 hPa. During the first SSW disturbance, the wavenumber 1 rapidly intensified, contributing the majority of the total eddy heat flux at the two pressure levels, followed by the sudden dip in the eddy heat flux due to the development of background easterly winds. During the second SSW, the total eddy heat flux increased rapidly at 100 hPa, and the contributions of wavenumber 1 and 2 were almost equal, while the contribution of wavenumber 2 was greater than the wavenumber 1 at 300 hPa. During the third SSW disturbance, the eddy heat flux was dominated by wavenumber 1 and 2 at 100 hPa. At 300 hPa, the eddy heat flux was comparably contributed by wavenumber 1, 2, and 3.

Figure 2 shows the 10 hPa polar vortex during six 100 hPa eddy heat flux peak periods. From 10 to 18 January 2024, due to the effect of wavenumber 1, the polar vortex was deformed and elongated. The polar vortex center (~29,000 gpm) was located near the Barents Sea, and the northwest European and North American continents showed correspondingly negative geopotential height anomalies. The high center (~31,500 gpm) was located over the Bering Strait, with corresponding positive geopotential height anomalies near the North Pole (Fig. 2a). From 28 January to 2 February, due to the combined effect of planetary wavenumber 1 and 2, the polar vortex was circular with a low center (~28,500 gpm) near the Severnaya Zemlya. Elongated negative height anomalies appeared in northern Eurasia and positive anomalies occurred over Greenland (Fig. 2b). From 11 to 19 February, the total eddy heat flux was enhanced compared to the previous stage, with equal contributions from wavenumber 1 and 2. The polar vortex evolved into an elliptical shape near the Kara Sea, and the negative geopotential height anomalies appeared accordingly (Fig. 2c). From 26 February to 2 March, the polar vortex became circular, with its center almost unchanged (Fig. 2d). From 3 to 8 March, with the onset of the third SSW, the polar vortex weakened and changed into an elliptical shape. The positive geopotential height anomalies were enhanced and occupied the polar region (Fig. 2e). From 9 to 14 March, the polar vortex continued to weaken and moved westward, with the high center and positive anomalies occupying the polar vortex (Fig. 2f). In short, all the three SSW events were displacement type, although the wavenumber 2 showed intermittent pulses.

Similarly, the 500 hPa height anomalies in the six peak periods with eddy heat flux pulses are shown in Fig. 3. During the first SSW from 10 to 18 January 2024, the geopotential height anomalies at mid- and high latitudes showed a wavenumber 2 pattern (Fig. 3a). From 28 January to 2 February, the geopotential height anomalies in midlatitudes were fairly large, showing a wavenumber 3 pattern (Fig. 3b). During the second minor SSW from 11 to 19 February, the geopotential height anomalies in midlatitudes weakened compared with the previous two periods, but the wavenumber 2 pattern and the climatological wavenumber 2 pattern were in sync (Fig. 3c). From 26 February to 2 March, the height anomalies in midlatitudes were very strong and showed a wavenumber 3 pattern. The positive anomalies in the Urals and the climatological wavenumber 1 and 2 were in sync, which amplified the tropospheric planetary waves (Fig. 3d). During the third SSW from 3 to 8 March, the high anomaly center in Urals moved towards the North Pole and intensified (Fig. 3e). From 9 to 14 March, the geopotential height anomalies in midlatitudes were very weak, presenting a wavenumber 1 pattern, accompanied by a weakening of tropospheric planetary wave activities (Fig. 3f).

Previous studies have shown that both following the elongation of the stratospheric polar vortex and after the SSW onset, large-scale cold air outbreaks may occur subsequently especially in North America[2,53,54]. The evolution of 2-m temperature anomalies in six subperiods during the three stratospheric disturbances is depicted in Fig. 4. From 2 to 12 January, cold anomalies appeared in northern Eurasia (center: ~−12 °C) and northern North America, and most of Eurasia was covered by the warm anomalies (Fig. 4a). From 13 to 23 January after the first SSW onset, strong cold anomalies (center: ~−12 °C) appeared in the North American continent, which were related to the polar vortex elongation during the SSW (Fig. 4b). From 24 January to 3 February, North America and northern Eurasia were covered by large warm anomalies, implying little downward impact from the stratosphere (Fig. 4c). From 4 to 14 February, warm anomalies persisted over most of North America and western Eurasia (Fig. 4d). From 15 to 25 February after the second SSW onset (albeit minor), central Eurasia was covered by cold anomalies (center: ~−10 °C), while North America was dominated by warm anomalies (Fig. 4e). From 26 February to 7 March, northwestern North America and central Eurasia were invaded by cold

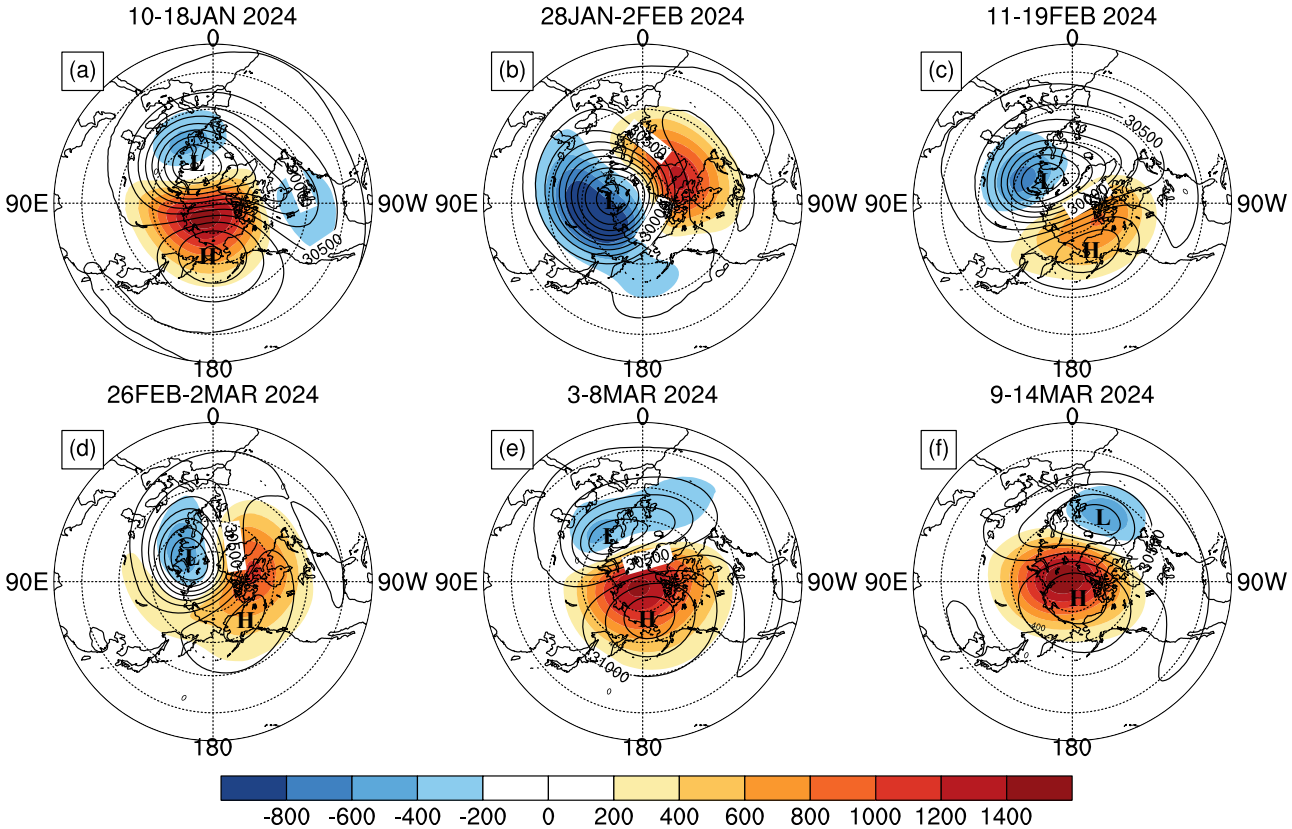

Fig. 2 | Synoptic maps of the 10 hPa geopotential heights (contour; unit: gpm) and their anomalies (shadings; unit: gpm) averaged in several subperiods. a The average from 10–18 January 2024. **b** The average from 28 January–2 February 2024. **c** The average from 11–19 February 2024. **d** The average from 26 February–2 March 2024. **e** The average from 3–8 March 2024. **f** The average from 9–14 March 2024. The letters H and L denote the high and low centers, respectively.

anomalies, while northern Eurasia and southeastern North America were covered by warm anomalies (Fig. 4f). From 8 to 18 March during the third SSW period (it lasted for longer time than the other two disturbances), most of Eurasia and North America showed warm anomalies (Fig. 4g). From 19 to 31 March, cold anomalies developed in central and northern North America, while warm anomalies appeared in Eurasia (Fig. 4h), consistent with the temperature anomaly patterns following SSW onset in previous studies[8,27].

Tropics-Arctic coupling during stratospheric disturbances in 2024

The BD circulation is a giant meridional circulation in the stratosphere, rising in the tropics and descending in the polar region[31–33]. With the BD circulation, stratospheric traces such as water vapor and ozone can complete tropics-pole transport and source-sink cycles[33,36]. In the lower stratosphere of the tropics, the zonal winds were in the QBO easterly phase in early 2024. Easterly anomalies (center: ~−14 m s^{-1}) appeared from 70 to 20 hPa, while westerly anomalies (center: ~16 m s^{-1}) appeared from 10 to 5 hPa. After the third SSW onset, the westerly anomalies intensified and propagated downwards (Fig. 5a). The zonal wind anomalies following the third major SSW onset are depicted in Fig. 5b. Over the Arctic large easterly anomalies were observed throughout the entire stratosphere with the anomaly center around 20–5 hPa (~−12 m s^{-1}). Corresponding to the easterly anomaly center, the lower stratosphere (center: ~−4 K) and upper stratosphere (center: ~−8 K) in the tropics were covered by cold anomalies (Fig. 5c). After the third SSW onset, the upper stratosphere in the polar region was covered by cold anomalies, while the middle and lower stratosphere were covered by warm anomalies (Fig. 5d).

The tropics is the main source region where water vapor enters the stratosphere from the troposphere. With the ascending branch of BD circulation, a large amount of water vapor is transported upward from the troposphere[39,40]. After freezing due to the lowest temperature layer near the tropopause, lots of water vapor falls back to the troposphere, and only a small part of water vapor enters the stratosphere[39,40]. In other words, the intensity of BD circulation dynamics and the tropopause cold point temperature affect the variation of tropical water vapor. The tropical water vapor content was higher in upper than lower stratosphere in early 2024. Following the third major SSW eruption, the water vapor content was lower than 2.2 ppm in lower stratosphere (Fig. 5e). According to the relative change of water vapor, the water vapor content in lower stratosphere began to decrease after the first SSW onset, explained by the drying effect of colder temperature. In contrast, the water vapor content in upper and middle stratosphere increased as compared with the climatology. This increase was related to the enhancement of the BD circulation, which overwhelmed the drying effect of colder temperature in regions where cold anomalies were relatively weaker than the tropopause. Following the third major SSW eruption, the water vapor at 70 hPa decreased by 8% relative to the climatology, whereas in mid- and high-latitudes, the lower stratospheric water vapor was about 8% higher than the climatology (Fig. 5g).

The stratospheric ozone content also shows similar variability to the water vapor in the tropics. The ozone was mostly localized in the upper stratosphere around 20–2 hPa, whereas the ozone content in the lower stratosphere was much lower (Fig. 5h). In terms of the relative ozone change in the tropics, the ozone was 7.5% less in the lower stratosphere than the long-term mean because the low temperature in the lower stratosphere was not conducive to the generation of ozone photochemical reaction[38], and the enhancement of the BD circulation during the SSW further amplified the negative ozone anomalies via vertical advection. The upper stratospheric ozone content was higher than the climatology with the maximum center

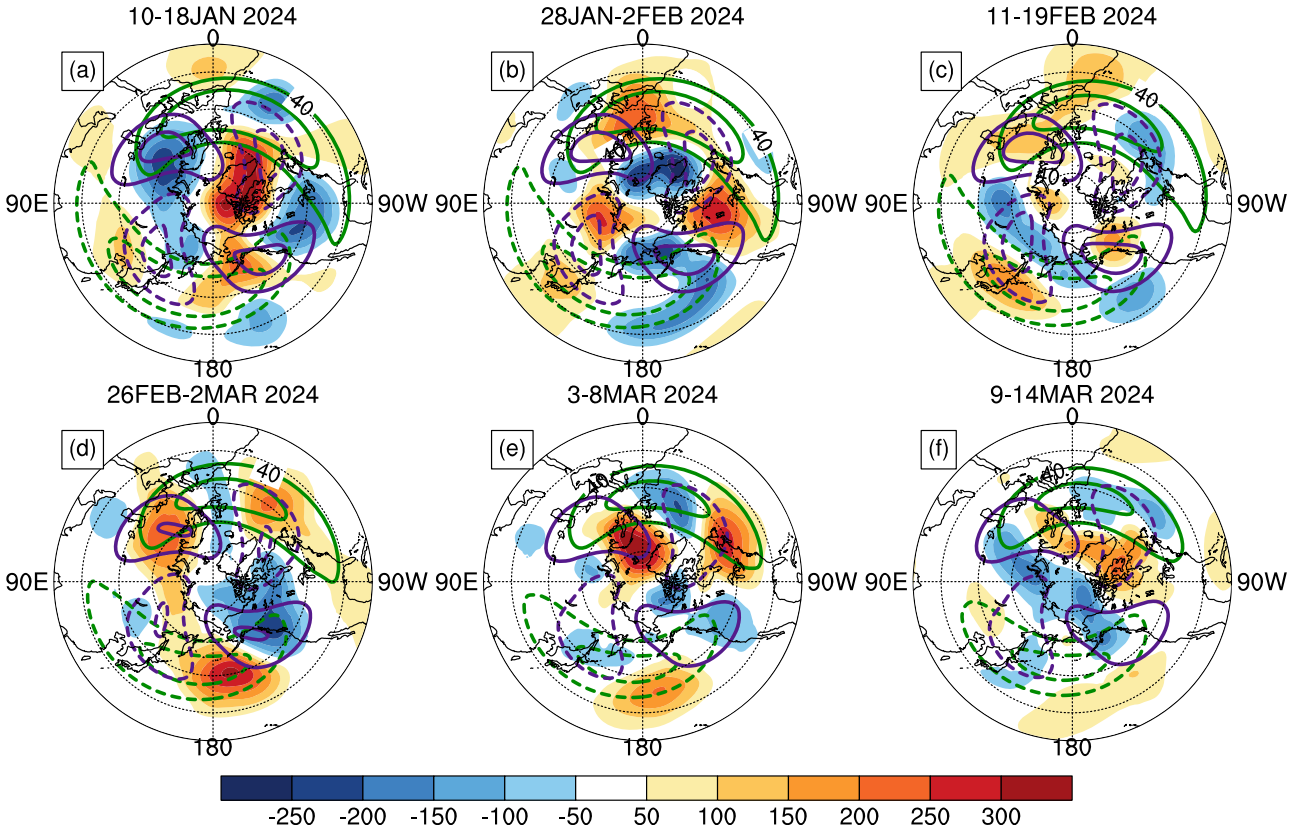

Fig. 3 | The 500 hPa height anomalies (shadings; unit: gpm) and climatological wavenumber 1 and 2 patterns (contour; unit: gpm) averaged in six subperiods. The green contours represent planetary wavenumber 1, and the purple contours represent planetary wavenumber 2. **a** The average from 10–18 January 2024. **b** The average from 28 January–2 February 2024. **c** The average from 11–19 February 2024. **d** The average from 26 February–2 March 2024. **e** The average from 3–8 March 2024. **f** The average from 9–14 March 2024.

~7.5%, mainly due to the transport of lower stratospheric ozone to this region (Fig. 5i).

The Arctic ozone and water vapor in the stratosphere are primarily sourced from the tropics where water vapor and ozone are rich[33]. Water vapor, ozone, and the BD circulation over the Arctic during the stratospheric disturbances are depicted in Fig. 6. Arctic water vapor was higher in the upper than lower stratosphere, showing similar distribution to the tropics. The water vapor content in the Arctic was much higher than in the tropics (Fig. 6a vs Fig. 5e). According to the relative water vapor change in the Arctic region, the lower stratospheric water vapor was 8% higher than the climatology below 50 hPa. Following the SSW eruption, the stratospheric water vapor anomaly center in the Arctic region descended. Following the third SSW, upper stratospheric water vapor was 4% less than the climatology, mainly due to the enhanced BD circulation during the SSW (Fig. 6b). According to 10 hPa water vapor anomalies, the tropical water vapor was higher than the climatology and exhibited enhanced poleward propagation especially after the SSW onset (Fig. 6c).

The high concentration of ozone in the Arctic region was mainly concentrated around 20–2 hPa, which was consistent with tropical regions, but Arctic ozone was lower than that in tropical regions (Fig. 6d). Following the SSW eruption (especially the third SSW), in middle and lower stratosphere, Arctic ozone exceeded the climatology. The ozone in the lower stratosphere was >20% higher than the climatology, which was attributed to the enhancement of the BD circulation. It was worth noting that after the first and third SSW, the upper stratospheric ozone content increased a lot, which was mainly attributed to the enhanced meridional advection of ozone from ozone-richer regions[38,55,56] (Fig. 6e). Due to the short interval between the second and the third SSW, the BD circulation was almost continuously enhanced during the two SSWs (Fig. 6g, h). From the spatial distribution of BD circulation (Fig. 6i), it was also obviously seen that there was a strong downdraft in the Arctic, and ozone was transported to the middle and lower stratosphere without staying in the upper stratosphere. After the first and third SSWs, the strengthening of BD circulation was followed by a weakening period, when the ozone transported to the Arctic was able to stay in the upper stratosphere. The high concentration of ozone in the tropics could gradually move to high latitudes, leading to subseasonal variability of ozone over the Arctic (Fig. 6f).

The intermittent enhancement of the poleward transport of water vapor and ozone was consistent with the BD circulation variations during the SSW onset. The residual circulation's vertical component in the polar regions showed obvious positive anomalies, indicating the sinking was accelerated when the SSW occurred (Fig. 6g). At the same time, the residual circulation's vertical component in the tropics clearly showed negative anomalies, indicating an enhanced upwelling (Fig. 6h). It was observed that the downwelling anomalies in the Arctic are 2 or 3 times larger than the upwelling anomalies in the tropics. A few days before the first SSW, enhanced wave forcing denoted by a strong eddy heat flux pulse (Fig. 1h) drove the strengthening of the BD circulation. The time average distribution of BD circulation anomalies from 9 February to 9 March is shown in Fig. 6i, which further indicates an enhanced tropics-Arctic coupling (Fig. 6i).

The background environment in the 2023/24 winter

Changes in the background environment can trigger or amplify tropospheric planetary waves, which propagate upwards and weaken polar vortex in the stratosphere. Arctic sea ice, ENSO, and some specific MJO phases are all likely factors that weaken polar vortex in the Arctic stratosphere[2,41,43,47]. Holton and Tan found that the polar vortex weakens (strengthens) when the

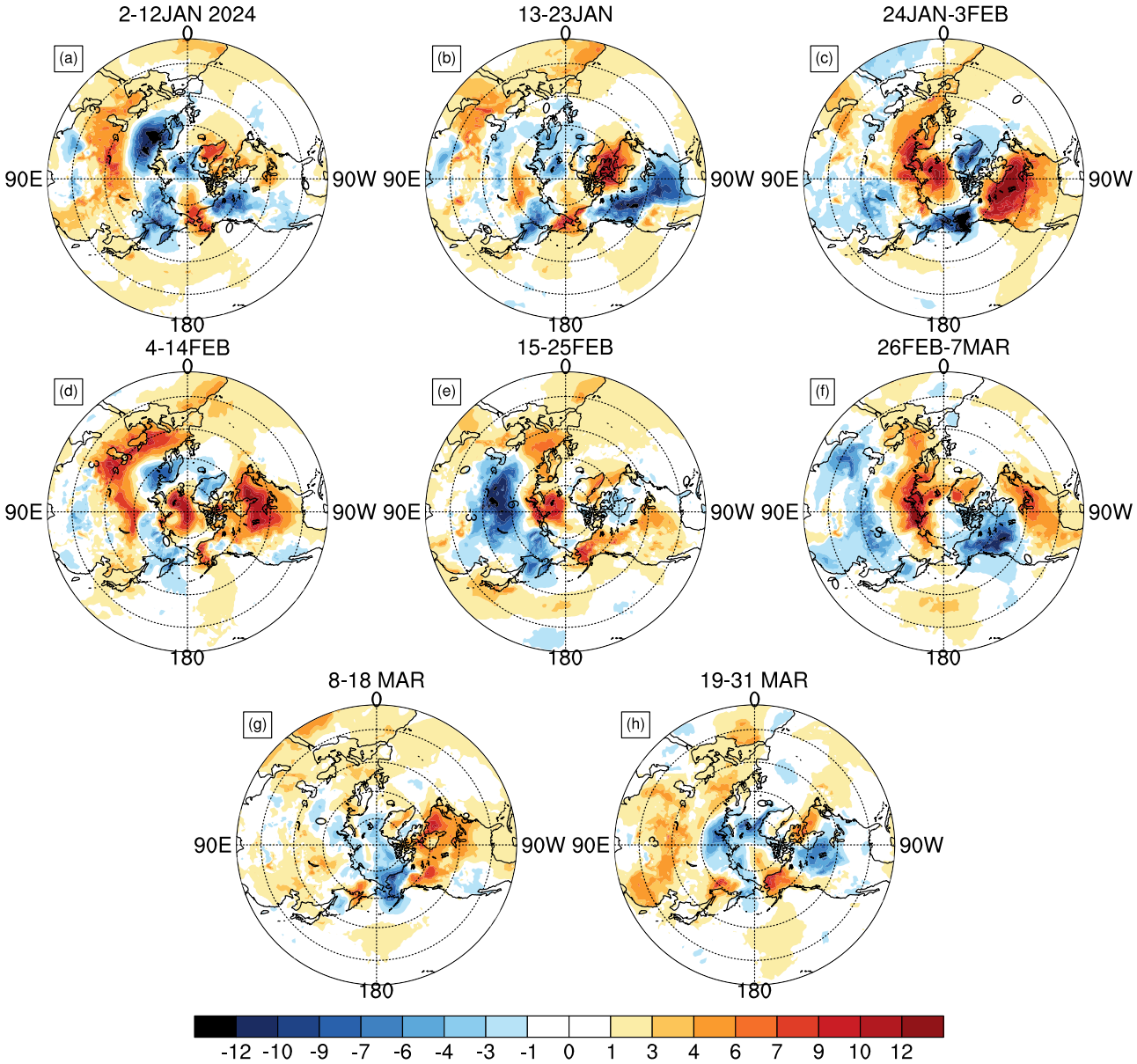

Fig. 4 | Synoptic maps of the 2-m temperature anomalies (unit: °C) averaged in eight subperiods. a The average from 2–12 January 2024. **b** The average from 13–23 January 2024. **c** The average from 24 January–3 February 2024. **d** The average from 4–14 February 2024. **e** The average from 15–25 February 2024. **f** The average from 26 February–7 March 2024. **g** The average from 8–18 March 2024. **h** The average from 19–31 March 2024.

tropical stratosphere is in the easterly (westerly) QBO phase[43,44]. All those potential factors controlling the stratospheric disturbances are analyzed.

During 2–15 January, a dozen days before the first SSW except for a few days, MJO was active in 3–4 phases with amplitudes exceeding one σ. During 1–15 February, two weeks before the second stratospheric disturbance, MJO appeared in 6–7 phases with an amplitude greater than 1.5σ. Before the third SSW onset, the MJO rapidly retreated from phase 6–7 to 3–4, and the amplitude exceeded one σ one week before the SSW onset. In other words, the two major SSWs occurred in the 3–4 phases of MJO and their amplitudes exceeded one σ (Fig. 7a).

The 3-year La Niña state ended in the 2023/24 winter[52], and the ENSO started a transition to an El Niño state, with the Niño 3.4 index reaching 2.0 °C. It can be seen that the sea surface temperature (SST) in the eastern and middle Pacific equatorial regions has undergone a rapid transition from cold to warm (Fig. 7b). On average, the warm SST in the tropical middle and eastern Pacific can trigger negative height anomalies in the troposphere over the North Pacific, which were also observed in January 2024 (the pattern correlation or PCC = 0.44, Fig. 8b) but weaker in February (PCC = 0.11, Fig. 8e). This strong Pacific-North American pattern response was beneficial to trigger and amplify the tropospheric climatological planetary waves, which propagated upward and weakened the stratospheric polar vortex.

Previous studies have reported Arctic sea ice loss especially in the Barents-Kara Sea can enhance the upward propagation of planetary waves and subsequently affect the intensity of the stratospheric polar vortex[49,57,58]. Table 1 shows the statistical relationship between detrend normalized BK sea ice index and major SSWs in winter from 1979/80 to 2023/24. SSWs occur in both years with sea ice growth and loss. No evidence shows that sea ice variability is related with increased SSW frequency, although models diverge in the stratospheric circulation responses to the BK sea ice loss[49,51,57–60]. The stratospheric signals associated with sea ice variability in several modeling studies are negligible[61–63]. The statistics from the observations show that the SSW frequency for sea ice growth and loss is comparable (Table 1). The weak sea ice growth in early 2024 was possibly not the responsible factor for the enhanced wave activities (Fig. 7c).

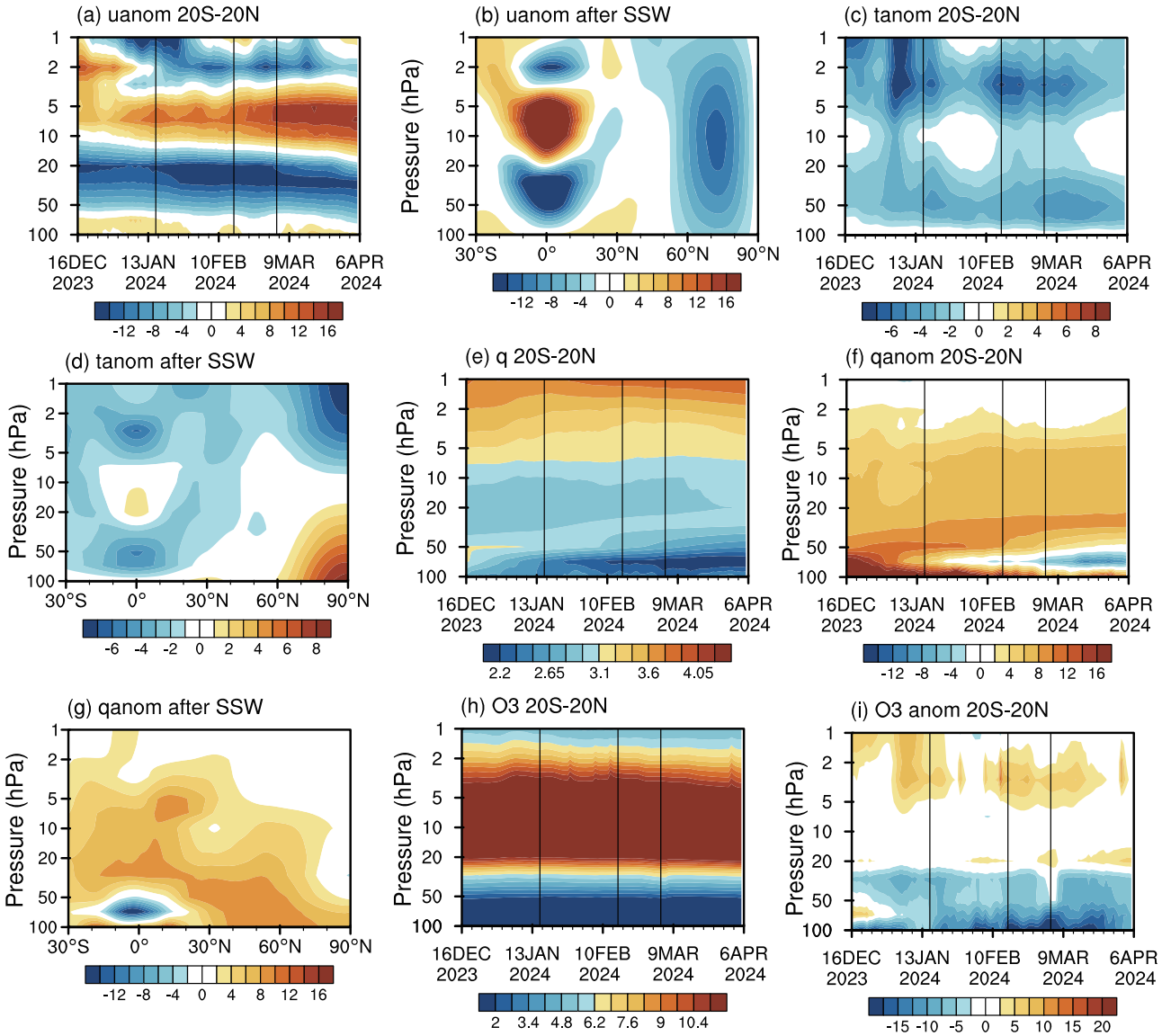

Fig. 5 | Spatiotemporal evolutions of zonal-mean or area-averaged (20°S–20°N) zonal winds, temperature, water vapor, and ozone in the tropics. **a** Zonal wind anomalies from 100–1 hPa (unit: m s^{-1}). **b** Zonal-mean zonal wind anomalies averaged from 4 March to 5 April (units: m s^{-1}). **c** Air temperature anomalies from 100–1 hPa (unit: K). **d** Zonal-mean air temperature anomalies averaged from 4 March to 5 April (unit: K). **e** Water vapor from 100–1 hPa (unit: ppm). **f** Relative change in water vapor compared to its climatology from 100–1 hPa (unit: %). **g** Zonal-mean relative change in water vapor averaged from 4 March to 5 April (unit: %). **h**, **i** As in (**e**, **f**), respectively, but for ozone.

The final potential factor that possibly contributed to the circulation variation analyzed is the QBO. The QBO was in the easterly phase in the 2023/24 winter when the 50 hPa QBO index is adopted (Fig. 7d). The composite height anomalies in QBO easterly winter revealed that the QBO-related circulation anomalies in January and February are positively associated with the height anomalies in January 2024 (PCC = 0.21, Fig. 8c) and February (PCC = 0.55, Fig. 8f) in 2024. Comparing the QBO with other controlling factors, the QBO easterly phase can explain more the three stratospheric disturbances in early 2024.

Conclusions

This study used ERA5 reanalysis, MJO index, sea ice and SST to analyze the primary characteristics of the stratosphere-troposphere and the tropics-Arctic couplings during three stratospheric disturbances in early 2024. In addition, the atmospheric and oceanic environments in the 2023/24 winter were also diagnosed. The main findings are as follows.

Three strong stratospheric disturbances occurred in the 2023/24 winter under special background conditions. On 16 January, a marginal major displacement SSW occurred in the stratosphere due to the high eddy heat flux pulse caused by planetary wavenumber 1. Although the easterlies at 60°N lasted for only two days, the positive geopotential height anomalies during this SSW propagated downward to the ground and exhibited the negative NAM pattern. On 16 February, a minor displacement SSW erupted because of the strong pulse of combined wavenumber 1 and wavenumber 2. Although the 80°N zonal-mean temperature was greater than 60°N, the 60°N zonal-mean zonal winds were still westerlies. The positive height anomaly signals propagated downward to the ground immediately after the minor SSW onset, but the duration period was very short. On 4 March, a major displacement SSW occurred in the stratosphere, which lasted for 21 days, due to the continuous upward propagation of planetary wavenumber 1 and 2. The positive height anomaly signal propagated downward to the near surface immediately following the major SSW, and then the

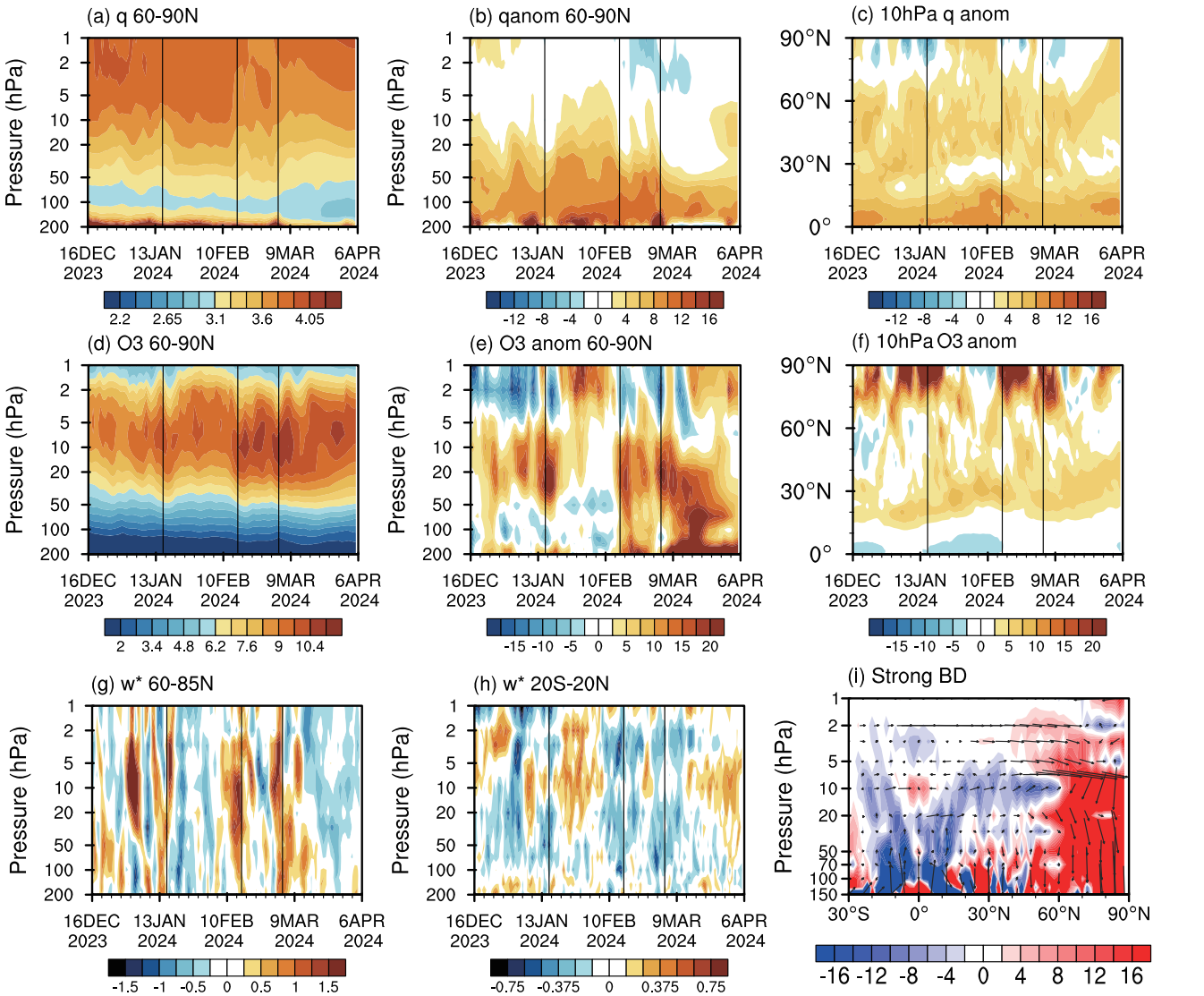

Fig. 6 | Spatiotemporal evolutions of zonal-mean or area-averaged (60°–90°N) water vapor, ozone, and the residual circulation. a Arctic water vapor from 200–1 hPa (unit: ppm). **b** Relative change in water vapor from 200–1 hPa compared with the climatology (unit: %). **c** Relative change in water vapor at 10 hPa. **d**, **e**, **f** As in (**a**, **b**, **c**) but for the polar cap ozone. **g** Polar cap mean vertical component of the standardized residual velocity. **h** As in (**g**) but for tropical residual velocity. **i** The residual circulation averaged from 9 February to 9 March (the vertical component is also highlighted in shadings).

positive anomalies covered the stratosphere and troposphere until early April.

The SSW disturbances in the stratosphere were closely related to the 2-m temperature anomalies variation on the near surface. Within ten days of the first SSW during 13–23 January, widespread cold anomalies with a center of −12 °C occurred over the North American continent, which were likely associated with downward propagation of the stratospheric disturbance signal. From 24 January to 14 February two weeks after the first SSW and before the second SSW when the stratospheric downward control seemed absent, North America and western Eurasia were covered by strong warm anomalies. From 15 February to 7 March after the second minor SSW onset, cold anomalies invaded northwestern North America and central Eurasia. From 19 to 31 March during the late stage of the third SSW, cold anomalies invaded the northern North American.

The QBO and strengthened BD circulation together directly affected ozone and water vapor in tropical regions. Although the 50 hPa QBO was in the easterly phase, the tropical zonal winds were characterized by easterly anomalies both in upper and lower stratosphere, and westerly anomalies in middle stratosphere, exhibiting a sandwich pattern. As a consequence, the corresponding temperatures were characterized by cold anomalies both in the top and bottom stratosphere. With the strengthened BD circulation during SSWs, more water vapor in the troposphere was transported to the stratosphere, leading to a rise in stratospheric water vapor in comparison to climatology. However, the tropical lower stratospheric temperature was colder following SSW onset, and corresponding local water vapor showed negative anomalies in the tropics. Because ozone was mainly concentrated in the stratosphere, both the strengthened BD circulation and colder temperature anomalies in lower stratosphere led to increased tropical ozone in upper stratosphere and decreased ozone in lower stratosphere.

Water vapor and ozone in the Arctic were mainly transported from the tropics with the enhanced BD circulation. During three observed stratospheric disturbances, the residual circulation was enhanced, exhibiting strengthened tropical upwelling and the accelerated Arctic downwelling. With the strengthened BD circulation, tropical ozone and water vapor were obviously transported poleward, explaining the positive change of ozone and water vapor in the Arctic. The downwelling over the Arctic further transported more traces from upper to lower stratosphere.

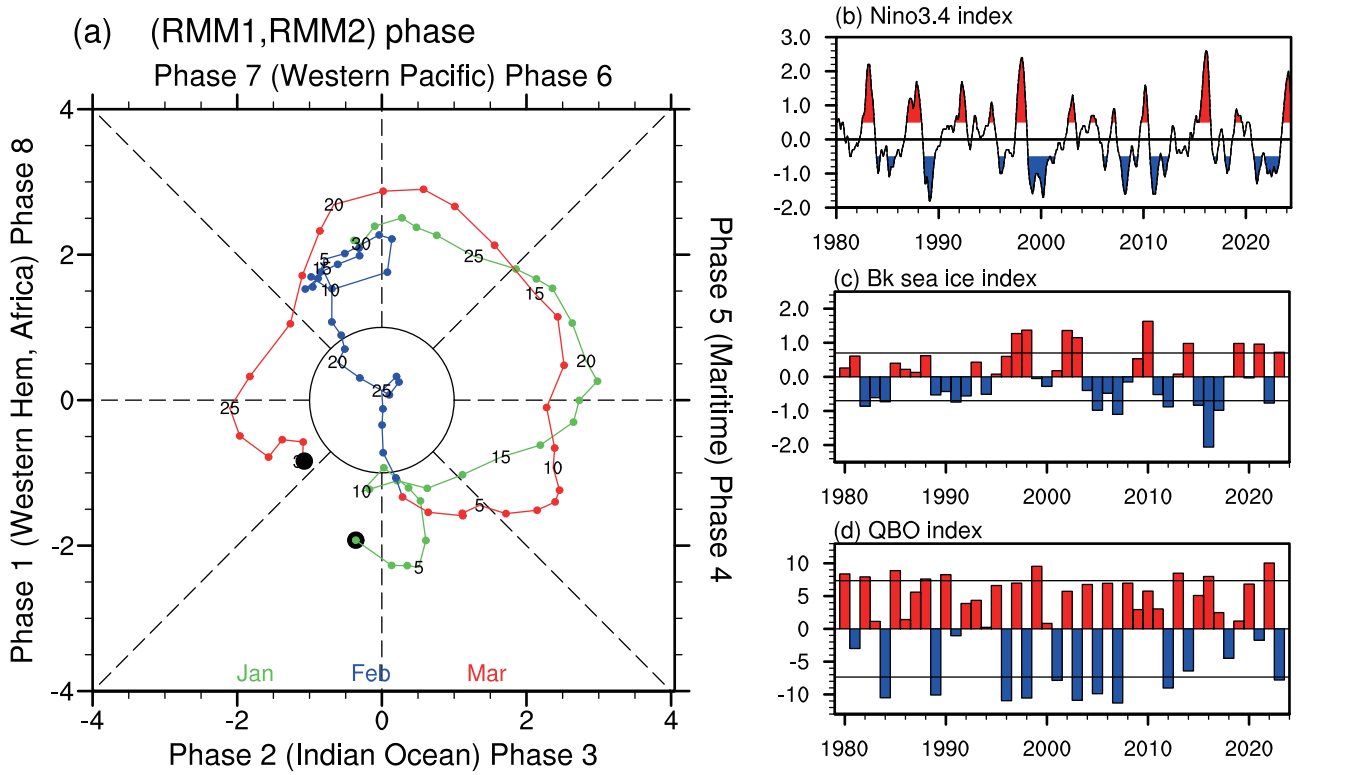

Fig. 7 | Backgrounds for the stratospheric disturbances in the 2023/24 winter. a MJO index in early 2024. **b** Timeseries of the Niño3.4 index from 1980 to the present (unit: °C). El Niño is highlighted in red, La Niña is highlighted in blue. **c** Timeseries of the normalized detrended sea ice index for the Barent-Kela Sea area (60–85°N, 10–110°E, BK) in winter from 1980 to the present, with horizontal lines indicating ±σ (0.7). **d** Timeseries of the 50 hPa QBO index in winter from 1980 to the present (unit: m/s), with horizontal lines representing ±σ (7.35).

Frequent stratospheric disturbances in the 2023/24 winter was possibly related to different driving forcings, including the warm tropical Pacific SST, the easterly QBO, and the active MJO. The SST in the equatorial east and middle Pacific changed rapidly from the La Niña to El Niño state, and the Niño 3.4 index even reached 2.0 °C in December 2023. The 50 hPa equatorial zonal winds was in the easterly QBO phase. A composite analysis reveals that the composite 500 hPa height anomalies both in January and in February for El Niño were present in the positive Pacific-North American pattern, highly resembling observed 500 hPa height anomaly pattern in January and February 2024. Before the two major SSWs onset, the MJO was active in the phase 3-4 with the amplitudes exceeding one σ. These climatic factors together triggered and enhanced the planetary wave activities in the troposphere, which finally propagated upward and weakened the stratospheric polar vortex.

The stratospheric disturbances have been observed to be anomalously more frequent in the past two winters. However, the question whether the global warming has reached a tipping point when the stratosphere is more easily disturbed is still not answered, left for a future study based on the model outputs.

Methods

Datasets

The European Centre for Medium Range Weather Forecasts provided the 5th Generation Reanalysis (ERA5) data, which covered the period from January 1979 to April 2024. The data had a latitude-longitude resolution of 1° × 1° and 37 vertical isobaric levels ranging from 1000 to 1 hPa[64]. The time resolution of the ERA5 reanalysis data we use is daily, calculated as the average of hourly data per day. Variables used include geopotential height, meridional and zonal winds, specific humidity, vertical velocity, and ozone mixing ratio at multiple isobaric levels, and 2-m temperature on the single level is also used.

The Met Office Hadley Centre (HadISST) provides monthly SST and sea ice concentration data from December 1979 to April 2024, with 1° (latitude) × 1° (longitude) horizontal resolution[65]. The Madden Julian Oscillation (MJO) index for January to March 2024 is provided by the Australian Bureau of Meteorology[66].

Methodology

The long-term mean for the period from 1979 to 2023 is used to compute the climatology. The difference between the daily climatology and the daily raw data is referred to as the anomaly for a certain variable.

In this study, the eddy heat flux ($\overline{v'T'}$) is calculated using daily air temperature and meridional wind. The overbar shows the zonal average, while the prime shows the zonal deviation[4]. The intensity of planetary waves propagation in the vertical direction is represented by the weighted average of the transient eddy heat flux over 45–75°N at 300 hPa and 100 hPa, where the vertical component of the Eliassen-Palm (E-P) flux (F_z) is nearly proportional to the transient eddy heat flux. Because only planetary waves have the ability to travel higher into the stratosphere[67], the eddy heat flux component generated by the wavenumbers 1–3 of the planetary wave is diagnosed.

The residual circulation's vertical and meridional residual velocities are calculated as follows:

$$\bar{v}^* = \bar{v} - \frac{\partial}{\partial P}\left(\frac{\overline{v'\theta'}}{\bar{\theta}_p}\right),$$

$$\bar{\omega}^* = \bar{\omega} - \frac{\partial}{r_0 \cos\varphi \partial\varphi}\left(\frac{\overline{v'\theta'}\cos\varphi}{\bar{\theta}_p}\right).$$

In the equation, v represents the zonal wind component, ω is the vertical wind component at p coordinates, θ denotes potential temperature, φ signifies latitude, r_0 stands for Earth's radius, and p indicates pressure. The

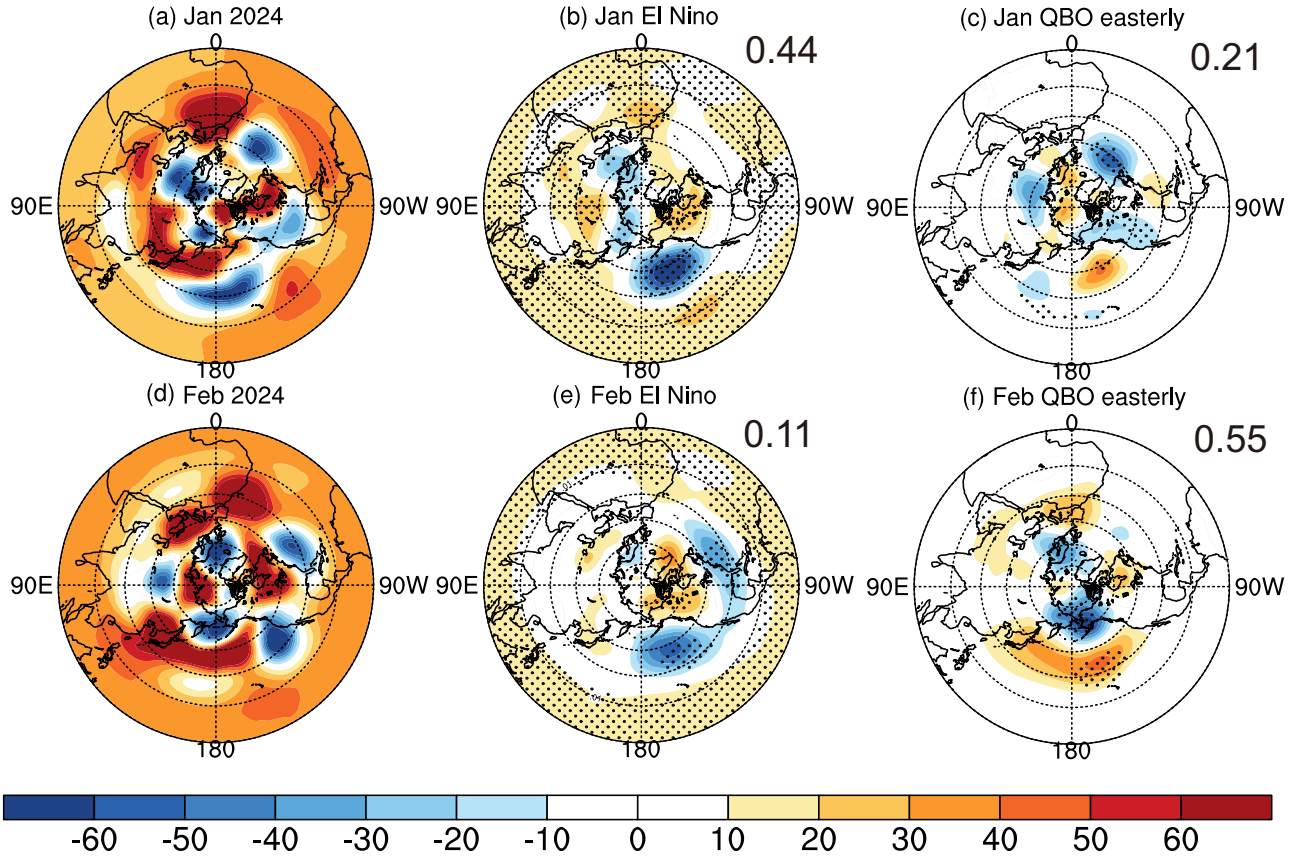

Fig. 8 | Possible attribution of the atmospheric circulation anomalies at 500 hPa. **a** Observed height anomalies in January 2024 (unit: gpm). **b** Composite height anomalies (unit: gpm) in January for 14 El Niño years (1983, 1987, 1988, 1992, 1995, 1998, 2003, 2005, 2007, 2010, 2015, 2016, 2019, 2024). **c** Composite height anomalies (unit: gpm) in January for 10 easterly QBO years (1985, 1990, 1997, 1999, 2002, 2004, 2006, 2008, 2013, 2024). **d**, **e**, **f** As in (**a**, **b**, **c**), respectively, but for the observed and composite anomalies in February. The pattern correlation between the 2024-observed and composite circulation anomalies are printed on the upper right if applicable. The black dots denote the composite anomalies at the 95% confidence level according to the two-sided *t*-test.

Table 1 | Relationship between detrend normalized BK sea ice index and major SSW in winter from 1979/80 to 2023/24

BK ice-SSW relationship			
BK ice phase	**Winter no.**	**SSW no.**	**SSW frequency**
BK ice growth (≥0.5σ)	15	8	0.53
BK ice loss (≤−0.5σ)	18	10	0.56
Neutral (|BKI| < 0.5σ)	12	9	0.75
Total	45	28	0.62

prime denotes zonal deviations, the overbar denotes zonal averaging, and the subscript p indicates differentiation with respect to pressure[33,36].

Reporting summary

Further information on research design is available in the Nature Portfolio Reporting Summary linked to this article.

Data availability

All data that support the findings of this study are included within the article or provided by the third parties. The data utilized in the study include 2-meter temperature data (https://doi.org/10.24381/cds.adbb2d47), circulation and temperature data (https://doi.org/10.24381/cds.bd0915c6) provided by the European Centre for Medium Range Weather Forecasts (ECMWF), sea ice and sea surface temperature distributed by the UKMO (https://www.metoffice.gov.uk/hadobs/hadisst/data/download.html), and the MJO RMM index provided by the BoM (http://www.bom.gov.au/clim_data/IDCKGEM000/rmm.74toRealtime.txt).

Code availability

The data in this study were analyzed and plotted with the NCAR Command Language (NCL) Version 6.6.2 (available at https://www.ncl. ucar.edu/). All relevant codes used in this study are available in the Zenodo repository[68] (https://doi.org/10.5281/zenodo.13925641).

Received: 23 June 2024; Accepted: 18 October 2024;
Published online: 26 October 2024

References

1. Baldwin, M. P. et al. Sudden stratospheric warmings. *Rev. Geophys.* **59**, e2020RG000708 (2021).
2. Lu, Q. et al. The sudden stratospheric warming in January 2021. *Environ. Res. Lett.* **16**, 084029 (2021).
3. Rao, J., Liu, S. & Chen, Y. Northern Hemisphere sudden stratospheric warming and its downward impact in four Chinese CMIP6 models. *Adv. Atmos. Sci.* **38**, 187–202 (2021).
4. Polvani, L. M. & Waugh, D. W. Upward wave activity flux as a precursor to extreme stratospheric events and subsequent anomalous surface weather regimes. *J. Clim.* **17**, 3548–3554 (2004).
5. Charney, J. G. & Drazin, P. G. Propagation of planetary-scale disturbances from the lower into the upper atmosphere. *J. Geophys. Res.* **66**, 83–109 (1961).
6. Butler, A. H. et al. Defining sudden stratospheric warmings. *Bull. Am. Meteorol. Soc.* **96**, 1913–1928 (2015).

7. Limpasuvan, V., Thompson, D. W. J. & Hartmann, D. L. The life cycle of the Northern Hemisphere sudden stratospheric warmings. *J. Clim.* **17**, 2584–2596 (2004).
8. Liang, Z., Rao, J., Guo, D. & Lu, Q. Simulation and projection of the sudden stratospheric warming events in different scenarios by CESM2-WACCM. *Clim. Dyn.* **59**, 3741–3761 (2022).
9. Charlton, A. J. & Polvani, L. M. A new look at stratospheric sudden warmings. Part I: climatology and modeling benchmarks. *J. Clim.* **20**, 449–469 (2007).
10. Cao, C. et al. Statistical characteristics of major sudden stratospheric warming events in CESM1-WACCM: a comparison with the JRA55 and NCEP/NCAR Reanalyses. *Atmosphere* **10**, 1–18 (2019).
11. Allen, D. R. et al. NOGAPS-ALPHA simulations of the 2002 Southern Hemisphere stratospheric major warming. *Mon. Weather Rev.* **134**, 498–518 (2006).
12. Shen, X., Wang, L. & Osprey, S. Tropospheric forcing of the 2019 Antarctic sudden stratospheric warming. *Geophys. Res. Lett.* **47**, e2020GL089343 (2020).
13. Seviour, W. J. M., Mitchell, D. M. & Gray, L. J. A practical method to identify displaced and split stratospheric polar vortex events. *Geophys. Res. Lett.* **40**, 5268–5273 (2013).
14. Rao, J., Garfinkel, C. I. & White, I. P. Predicting the downward and surface influence of the February 2018 and January 2019 sudden stratospheric warming events in subseasonal to seasonal (S2S) models. *J. Geophys. Res. Atmos.* **125**, e2019JD031919 (2020).
15. Yoden, S., Yamaga, T., Pawson, S. & Langematz, U. A composite analysis of the stratospheric sudden warmings simulated in a perpetual January integration of the Berlin TSM GCM. *J. Meteorol. Soc. Japan* **77**, 431–445 (1999).
16. de La Cámara, A., Birner, T. & Albers, J. R. Are sudden stratospheric warmings preceded by anomalous tropospheric wave activity? *J. Clim.* **32**, 7173–7189 (2019).
17. Boljka, L. & Birner, T. Tropopause-level planetary wave source and its role in two-way troposphere–stratosphere coupling. *Weather Clim. Dyn.* **1**, 555–575 (2020).
18. Ren, R. C. & Cai, M. Meridional and vertical out-of-phase relationships of temperature anomalies associated with the Northern Annular Mode variability. *Geophys. Res. Lett.* **34**, 1–4 (2007).
19. Baldwin, M. P. & Dunkerton, T. J. Stratospheric harbingers of anomalous weather regimes. *Science* **294**, 581–584 (2001).
20. Baldwin, M. P. & Thompson, D. W. J. A critical comparison of stratosphere–troposphere coupling indices. *Q. J. R. Meteorol. Soc.***135**, 1661–1672 (2009).
21. Karpechko, A. Y., Charlton-Perez, A., Balmaseda, M., Tyrrell, N. & Vitart, F. Predicting sudden stratospheric warming 2018 and its climate impacts with a multimodel ensemble. *Geophys. Res. Lett.* **45**, 13,538–13,546 (2018).
22. Thompson, D. W. J., Baldwin, M. P. & Wallace, J. M. Stratospheric connection to Northern Hemisphere wintertime weather: Implications for prediction. *J. Clim.* **15**, 1421–1428 (2002).
23. Yu, Y., Ren, R. & Cai, M. Dynamic linkage between cold air outbreaks and intensity variations of the meridional mass circulation. *J. Atmos. Sci.* **72**, 3214–3232 (2015).
24. Kolstad, E. W., Breiteig, T. & Scaife, A. A. The association between stratospheric weak polar vortex events and cold air outbreaks in the Northern Hemisphere. *Q. J. R. Meteorol. Soc.* **136**, 886–893 (2010).
25. Garfinkel, C. I., Son, S. W., Song, K., Aquila, V. & Oman, L. D. Stratospheric variability contributed to and sustained the recent hiatus in Eurasian winter warming. *Geophys. Res. Lett.* **44**, 374–382 (2017).
26. Rao, J. & Garfinkel, C. I. CMIP5/6 models project little change in the statistical characteristics of sudden stratospheric warmings in the 21st century. *Environ. Res. Lett.* **16**, 034024 (2020).
27. Lu, Q. et al. Possible influence of sudden stratospheric warmings on the atmospheric environment in the Beijing-Tianjin-Hebei region. *Atmos. Chem. Phys.* **22**, 13087–13102 (2022).
28. Lu, Q. et al. Observational subseasonal variability of the PM2.5 concentration in the Beijing-Tianjin-Hebei area during the January 2021 sudden stratospheric warming. *Adv. Atmos. Sci.* **39**, 1623–1636 (2022).
29. Lu, Q., Rao, J., Guo, D., Yu, M. & Yu, Y. Downward propagation of sudden stratospheric warming signals and the local environment in the Beijing-Tianjin-Hebei region: a comparative study of the 2018 and 2019 winter cases. *Atmos. Res.* **254**, 105514 (2021).
30. Huang, W., Yu, Y., Yin, Z., Chen, H. & Gao, M. Appreciable role of stratospheric polar vortex in the abnormal diffusion of air pollutant in North China in 2015/2016 winter and implications for prediction. *Atmos. Environ.* **259**, 118549 (2021).
31. Brewer, A. W. Evidence for a world circulation provided by the measurements of helium and water vapor distribution in the stratosphere. *Q. J. R. Meteorol. Soc.* **75**, 351–363 (1949).
32. Dobson, G. M. B. Origin and distribution of the polyatomic molecules in the atmosphere. *Proc. R. Soc. Lond. Ser. A. Math. Phys. Sci.* **236**, 187–193 (1956).
33. Butchart, N. The Brewer-Dobson circulation. *Rev. Geophys.* **52**, 157–184 (2014).
34. Holton, J. R., Haynes, P. H., Mcintyre, M. E., Douglass, A. R. & Rood, B. Stratonsphere-troposphere exchange. *Rev. Geophys.* **33**, 403–439 (1995).
35. Sato, K. & Hirano, S. The climatology of the Brewer-Dobson circulation and the contribution of gravity waves. *Atmos. Chem. Phys.* **19**, 4517–4539 (2019).
36. Hardiman, S. C., Butchart, N. & Calvo, N. The morphology of the Brewer-Dobson circulation and its response to climate change in CMIP5 simulations. *Q. J. R. Meteorol. Soc.* **140**, 1958–1965 (2014).
37. Haynes, P. H., Marks, C. J., Mcintyre, M. E., Shepherd, T. G. & Shine, K. P. On the "Downward Control", of extratropical diabatic circulations by eddy-induced mean zonal forces. *J. Atmos. Sci.* **48**, 651–678 (1991).
38. de La Cámara, A., Abalos, M., Hitchcock, P., Calvo, N. & Garcia, R. R. Response of Arctic ozone to sudden stratospheric warmings. *Atmos. Chem. Phys.* **18**, 16499–16513 (2018).
39. Li, F. & Newman, P. Stratospheric water vapor feedback and its climate impacts in the coupled atmosphere–ocean Goddard Earth observing system chemistry-climate model. *Clim. Dyn.* **55**, 1585–1595 (2020).
40. Smith, J. W., Bushell, A. C., Butchart, N., Haynes, P. H. & Maycock, A. C. The effect of convective injection of ice on stratospheric water vapor in a changing climate. *Geophys. Res. Lett.* **49**, e2021GL097386 (2022).
41. Rao, J., Garfinkel, C. I., Chen, H. & White, I. P. The 2019 new year stratospheric sudden warming and its real-time predictions in multiple S2S models. *J. Geophys. Res. Atmos.* **124**, 11155–11174 (2019).
42. Anstey, J. A. et al. Impacts, processes and projections of the quasi-biennial oscillation. *Nat. Rev. Earth Environ.* **3**, 588–603 (2022).
43. Baldwin, M. P. et al. The quasi-biennial oscillation. *Rev. Geophys.* **39**, 179–229 (2001).
44. Holton, J. R. & Tan, H.-C. The infuence of the equatorial Quasi-Biennial oscilation on the global circulation at 50 mb. *J. Atmos. Sci.* **37**, 2200–2208 (1980).
45. Andrews, M. B. et al. Observed and simulated teleconnections between the stratospheric Quasi-Biennial Oscillation and northern Hemisphere winter atmospheric circulation. *J. Geophys. Res. Atmos.* **124**, 1219–1232 (2019).
46. Ruzmaikin, A., Feynman, J., Jiang, X. & Yung, Y. L. Extratropical signature of the quasi-biennial oscillation. *J. Geophys. Res. D Atmos.* **110**, D11111 (2005).

47. Rao, J., Ren, R., Chen, H., Yu, Y. & Zhou, Y. The stratospheric sudden warming event in February 2018 and its prediction by a climate system model. *J. Geophys. Res. Atmos.* **123**, 13,332–13,345 (2018).
48. Garfinkel, C. I., Feldstein, S. B., Waugh, D. W., Yoo, C. & Lee, S. Observed connection between stratospheric sudden warmings and the Madden-Julian Oscillation. *Geophys. Res. Lett.* **39**, 1–5 (2012).
49. Screen, J. A. Simulated atmospheric response to regional and pan-arctic sea ice loss. *J. Clim.* **30**, 3945–3962 (2017).
50. Kim, B. M. et al. Weakening of the stratospheric polar vortex by Arctic sea-ice loss. *Nat. Commun.* **5**, 1–8 (2014).
51. Sun, L., Deser, C. & Tomas, R. A. Mechanisms of stratospheric and tropospheric circulation response to projected Arctic sea ice loss. *J. Clim.* **28**, 7824–7845 (2015).
52. Lu, Q. et al. Stratosphere-troposphere coupling during stratospheric extremes in the 2022/23 winter. *Weather Clim. Extrem*. **42**, 100627 (2023).
53. Cohen, J., Agel, L., Barlow, M., Garfinkel, C. I. & White, I. Linking Arctic variability and change with extreme winter weather in the United States. *Science* **373**, 1116–1121 (2021).
54. Ding, X., Chen, G., Zhang, P., Domeisen, D. I. V. & Orbe, C. Extreme stratospheric wave activity as harbingers of cold events over North America. *Commun. Earth Environ.* **4**, 1–10 (2023).
55. Hong, H. J. & Reichler, T. Local and remote response of ozone to Arctic stratospheric circulation extremes. *Atmos. Chem. Phys.* **21**, 1159–1171 (2021).
56. Shams, S. B. et al. Analyzing ozone variations and uncertainties at high latitudes during sudden stratospheric warming events using MERRA-2. *Atmos. Chem. Phys.* **22**, 5435–5458 (2022).
57. Kim, B.-M. et al. Weakening of the stratospheric polar vortex by Arctic sea-ice loss. *Nat. Commun.* **5**, 4646 (2014).
58. Xu, M. et al. Influence of regional sea ice loss on the Arctic stratospheric polar vortex. *J. Geophys. Res. Atmos.* **129**, e2023JD040571 (2024).
59. England, M., Polvani, L. & Sun, L. Contrasting the Antarctic and Arctic atmospheric responses to projected sea ice loss in the late twenty-first century. *J. Clim.* **31**, 6353–6370 (2018).
60. Cai, D., Dameris, M., Garny, H. & Runde, T. Implications of all season Arctic sea-ice anomalies on the stratosphere. *Atmos. Chem. Phys.* **12**, 11819–11831 (2012).
61. Dai, A. & Song, M. Little influence of Arctic amplification on mid-latitude climate. *Nat. Clim. Change* **10**, 231–237 (2020).
62. Smith, D. M. et al. Robust but weak winter atmospheric circulation response to future Arctic sea ice loss. *Nat. Commun.* **13**, 727 (2022).
63. Sun, L., Deser, C., Simpson, I. & Sigmond, M. Uncertainty in the winter tropospheric response to Arctic sea ice loss: the role of stratospheric polar vortex internal variability. *J. Clim.* **35**, 3109–3130 (2022).
64. Hersbach, H. et al. The ERA5 global reanalysis. *Q. J. R. Meteorol. Soc.* **146**, 1999–2049 (2020).
65. Rayner, N. A. et al. Global analyses of sea surface temperature, sea ice, and night marine air temperature since the late nineteenth century. *J. Geophys. Res. Atmos*. **108**, D14, 4407 (2003).
66. Wheeler, M. C. & Hendon, H. H. An all-season real-time multivariate MJO index: development of an index for monitoring and prediction. *Mon. Weather Rev.* **132**, 1917–1932 (2004).
67. Nishii, K., Nakamura, H. & Miyasaka, T. Modulations in the planetary wave field induced by upward-propagating Rossby wave packets prior to stratospheric sudden warming events: a case-study. *Q. J. R. Meteorol. Soc.* **135**, 39–52 (2009).
68. Lu, Q. Enhanced stratosphere-troposphere and tropics-Arctic couplings in the 2023/24 winter. *Zenodo* https://doi.org/10.5281/zenodo.13925641 (2024).

Acknowledgements

We acknowledge the Natural Science Foundation of China (NSFC) for funding (grant nos. 42322503, 42361144843, and 42175069) and NOAA, ECMWF, as well as ESGF for freely providing the relevant datasets. This work was also funded by Chengde Basic Research Project (202205B065), and 2023 Innovation Plan Project of Jiangsu Province (KYCX23_1303) also provide funding.

Author contributions

Q.L. performed the data analysis and prepared all figures. J.R. conceptualized the study. Q.L. and J.R. wrote the manuscript. C.S., R.R., and S.L. reviewed the manuscript.

Competing interests

The authors declare no competing interests.

Additional information

Supplementary information The online version contains supplementary material available at https://doi.org/10.1038/s43247-024-01812-x.

Correspondence and requests for materials should be addressed to Jian Rao.

Peer review information *Communications Earth & Environment* thanks Siddarth Shankar Das and the other, anonymous, reviewer(s) for their contribution to the peer review of this work. Primary Handling Editors: Kyung-Sook Yun and Alireza Bahadori. A peer review file is available.

Reprints and permissions information is available at http://www.nature.com/reprints

Publisher's note Springer Nature remains neutral with regard to jurisdictional claims in published maps and institutional affiliations.

Open Access This article is licensed under a Creative Commons Attribution-NonCommercial-NoDerivatives 4.0 International License, which permits any non-commercial use, sharing, distribution and reproduction in any medium or format, as long as you give appropriate credit to the original author(s) and the source, provide a link to the Creative Commons licence, and indicate if you modified the licensed material. You do not have permission under this licence to share adapted material derived from this article or parts of it. The images or other third party material in this article are included in the article's Creative Commons licence, unless indicated otherwise in a credit line to the material. If material is not included in the article's Creative Commons licence and your intended use is not permitted by statutory regulation or exceeds the permitted use, you will need to obtain permission directly from the copyright holder. To view a copy of this licence, visit http://creativecommons.org/licenses/by-nc-nd/4.0/.

© The Author(s) 2024